Electronic Supplementary Information for

The detailed characterization of electrochemically switchable molecular assemblies on silicon electrodes

Simone Ciampi,[a] *Michael James,*[b] *Moinul H. Choudhury,*[a] *Nadim Darwish,*[a] *J. Justin Gooding*[a]*

[a]School of Chemistry and the Australian Centre for NanoMedicine, University of New South Wales, Sydney 2052, Australia

[b]Australian Nuclear Science and Technology Organisation (ANSTO), Locked Bag 2001, Kirrawee DC 2232, Australia

S1. Experimental Section

S1.1 Chemicals

All chemicals, unless specified otherwise, were of analytical grade and used as received. Chemicals used in surface modification procedures and electrochemical experiments were of high purity (≥ 99%). Hydrogen peroxide (30 wt % sol. in water, Sigma-Aldrich), hydrofluoric acid (Riedel-de Haën, 48 wt % sol. in water), and sulfuric acid (J. T. Baker) used in wafers cleaning and etching procedures were of semiconductor grade. 1,8-Nonadiyne (**1**, Alfa Aesar, 97%) was redistilled from sodium borohydride (Sigma-Aldrich, 99+%) under reduced pressure (80 ºC, 10−12 Torr) and stored under a high purity argon atmosphere (H_2O < 10 ppb, O_2 < 5 ppb) prior to use. Milli-Q™ water (> 18 MΩ cm) was used to prepare solutions and for chemical reactions. Dichloromethane, chloroform, hexane, light petroleum (b.p. 60−80 ºC), acetone, tetrahydrofuran, 2-propanol, ethanol, methanol and ethyl acetate for chemical reactions, surface cleaning procedures and purification procedures were redistilled

prior to use. The drying of solvents used in chemical reactions was as follows: (a) carbon tetrachloride was distilled from phosphorus pentoxide; (b) dichloromethane was distilled from calcium hydride; (c) diethyl ether was distilled from sodium using a benzophenone indicator; (d) *N,N*-dimethylformamide was distilled under reduced pressure from calcium hydride; (e) 1,4-dioxane was distilled from sodium; (f) ethanol was distilled from sodium; (g) 2-propanol was distilled from sodium; (h) pyridine was distilled under reduced pressure from potassium hydroxide; (i) tetrahydrofuran was distilled from sodium using a benzophenone indicator; (l) toluene was distilled under reduced pressure from calcium hydride. *p*-Toluensulfonyl chloride (Sigma-Aldrich, 98%) was recrystallized from chloroform/hexane. Sodium azide (Sigma-Aldrich, 98%) was crystallized from water by the addition of ethanol. β,β-Dimethylacrylic acid (Sigma-Aldrich, 97%) was recrystallized from light petroleum. Thin-layer chromatography (TLC) was performed on Merck silica gel aluminum sheets (60 F254). Davisil®LC 60 Å silica gel (40−60μm) was used for column chromatography.

S1.2 Silicon wafers

Prime grade double-side polished silicon wafers, 100-oriented (<100> ± 0.9°), p-type (boron-doped), 500 ± 25 μm thick, 0.007–0.009 Ω cm resistivity, were obtained from Virginia Semiconductors, Inc. (VA, USA). Prime grade double-side polished silicon wafers, 100-oriented (<100> ± 0.05°), n-type (phosphorous-doped), 500 ± 25 μm thick, 0.0014–0.0018 Ω cm resistivity, were obtained from Siltronix, S.A.S. (Archamps, France).

S1.3 Surface analysis

S1.3.1 XPS measurements

X-ray photoelectron spectra were obtained on an ESCALAB 220iXL spectrometer fitted with a monochromatic Al Kα source (1486.6 eV), a hemispherical analyzer and a 6 channel detector. Spectra of Br 3d (62–78 eV binding energy), Si 2p (93–109 eV), C 1s (279–295 eV), N 1s (392–408 eV), O 1s (525–541 eV), F 1s (677–694 eV). Fe 2p (700–735 eV), and

Cu 2p (925–960 eV) as well as survey scans (0–1300 eV) were recorded in normal emission (θ = 90°) with the analyzing chamber operating below 10^{-9} mbar. The atomic compositions were corrected for atomic sensitivities and measured from high-resolution scans. Atomic sensitivity factors are often instrument-sensitive and so the atomic sensitivities obtained from the Avance software interfaced with the spectrometer were 2.840 for Br 3d, 0.817 for Si 2p, 1.000 for C 1s, 1.800 for N 1s, 2.930 for O 1s, 4.430 for F 1s, 16.420 for Fe 2p, 25.390 for Cu 2p. The resolution of the spectrometer is *ca*. 0.6 eV as measured from the Ag $3d_{5/2}$ signal (full width at half maximum, fwhm) with 20 eV pass energy. High-resolution scans were run with 0.1 eV step size, dwell time of 100 ms and the analyzer pass energy set to 20 eV. Survey scans were carried out over 1300−0 eV range with a 1.0 eV step size, a 100 ms dwell time and analyzer pass energy of 100 eV. After background subtraction using the Shirley routine, spectra were fitted with Voigt functions (a convolution of Lorentzian and Gaussian profiles) as described previously.[1, 2] Unless stated otherwise, all energies are binding energies expressed in eV, obtained by applying to all samples a rigid shift to bring the binding energy of the C 1s peak to a value of 285.0 eV. When detectable above noise levels, the fractional monolayer coverage of oxidized silicon was calculated directly from the oxidized-to-bulk Si 2p peak area ratio according to the method described by Webb and co-workers for very thin oxide overlayers.[3] The spectrometer silica detection limit can be approximated to *ca*. 0.06 monolayers equivalents. The ratios of the integrated areas for the C 1s and N 1s emissions, each normalized for their elemental sensitivity, scanning time (number of scans accumulated), and for a square root dependence on the photoelectron kinetic energy, afforded an estimate of the conversion of the acetylenyl surface (**SAM-1**) to the lactone-functionalized surface (**SAM-2**). Analogous quantitative considerations for the Fe 2p, C 1s and N 1s signals aided in the understanding of both the adsorbate stoichiometry at the different stages of film growth, as well as assisting in probing the outcome of the electrochemical cleaving processes.

S1.3.2 X-ray reflectometry

X-ray reflectivity (XRR) profiles of the self-assembled surfaces were measured under ambient conditions on a Panalytical Ltd X'Pert Pro Reflectometer using Cu Kα X-ray radiation (λ = 1.54056 Å). The X-ray beam was focused using a Göbel mirror and collimated with 0.2 mm pre-sample slit and a post-sample parallel plate collimator. Reflectivity data were collected over the angular range $0.05° \leq \theta \leq 5.00°$, with a step size of 0.010° and counting times of 10 s per step. Prior to measurements, samples were stored under argon and exposed to air for approximately 10 min in order to be aligned on the reflectometer. From the experimental data, structural parameters of the self-assembled structures were refined using the MOTOFIT analysis software with reflectivity data presented as a function of the momentum transfer vector normal to the surface $Q = 4\pi(\sin\theta)/\lambda$.[4] The Levenberg-Marquardt method was used to minimize $\chi 2$ values in the fitting routines. Single-layer or two-layer models were used to fit the observed data.

S1.3.3 Spectroscopic ellipsometry

Ellipsometric spectra were recorded using a variable angle spectroscopic ellipsometer (M-2000X-210, J. A. Woollam Co., Inc., USA) at three different angles of incidence (65°, 70°, and 75° to the surface normal) over the 250–1000 nm wavelength range (4.96–1.24 eV). The values of refractive index (n) and imaginary refractive index (k) for bare (*i.e.*, Si–H) phosphorous- and boron-doped reference substrates were taken before analysis. Acquired data on the changes in light polarization at the air/monolayer/substrate interfaces were modeled using the Cauchy approximation in the *WVASE 32*® software package, and were used to extract monolayer thickness values. Measurements of at least four different points on each surface were carried out and were found to be within 1 Å of the reported average. The sample-to-sample reproducibility was within 2 Å.

S1.3.4 Electrochemical characterization

Electrochemical experiments were performed in a PTFE three-electrode cell with the modified silicon surface as the working electrode, a platinum mesh (*ca*. 1200 mm^2) as the counter electrode, and Ag|AgCl in 3 M NaCl as the reference electrode. All potentials are reported versus the reference electrode. A rectilinear cross-section Viton® gasket defined the geometric area of the working electrode to 24.6 mm^2. Samples analyzed by electrochemical methods and successively used in either XRR or ellipsometry experiments had a size of 40 × 10 mm or 15 × 10 mm, respectively. The bulk of the back-side of the silicon sample was exposed with emery paper and rubbed with gallium indium eutectic. A planar copper electrode pressed to the sample backside served as an ohmic contact. The cell was enclosed in a grounded Faraday cage during all measurements. Electrochemical experiments at potentials more cathodic of –400 mV were conducted in degassed electrolytes (by means of bubbling argon gas for a minimum of 20 min) under continuos flow of argon. Cyclic voltammetry (CV) measurements were performed using a BAS 100B electrochemical analyzer (Bioanalytical Systems, Inc., W. Lafayette, IN). Electrochemical impedance measurements (EIS) were performed with a Solartron 1255B (Farnborough, UK) frequency response analyzer interfaced to a Solartron 1287 potentiostat/galvanostat module. Impedance data were collected at 60 frequencies in the frequency range of 0.01 Hz to 0.1 MHz. An ac potential amplitude of 15 mV root mean square was added to the dc potential (E_{dc}) of the working electrode. EIS measurements for ferrocenyl films (**SAM-5a/b**) were performed in aqueous perchlorate-based electrolytes. Both the in-phase (Z') and out-of-phase impedance (Z'') were extracted at the same time from the data and analyzed with the *ZView 3.1* and *ZPlot* softwares (Scribner Associates, Inc.). The formalism developed by Laviron was used to obtain kinetic information,[5] namely the apparent electron-transfer rate constant, k°_{et}, for the electron-

transfer process between tethered redox groups and the conducting substrate. All electrochemical experiments were performed at room temperature (23 ± 2 °C) in air.

S1.4 Synthetic procedures

The synthetic procedure for the preparation of the redox-sensitive lactone linker **2** in ten steps from commercially available 2,5-dimethylphenol has been reported elsewhere.[6] Linker molecules **3a** and **3b** were prepared from their immediate bromo and chloro precursors in a one-step procedure as reported previously.[7] Ethynylferrocene **4** was prepared in a two-step procedure (Scheme S1) from commercially available acetylferrocene following literature procedures with minor modifications (*vide infra*).[8] Unless otherwise specified NMR spectra were recorded on a Bruker Avance 300 spectrometer in deuteriochloroform ($CDCl_3$ from Aldrich, passed through basic alumina) using the solvent signal as an internal reference. FTIR spectra were recorded on a Thermo Nicolet Avatar 370 FTIR spectrometer by accumulating a minimum of 32 scans and selecting a resolution of 2 cm^{-1}.

The assembly of the redox-tagged and redox-switchable **SAM-5** followed the synthetic procedures depicted in Scheme 2 and is detailed in the following section. The dormant[9] lactone linker molecule **2** was attached to acetylenyl Si(100) surfaces (**SAM-1**) through a Cu(I)-catalyzed alkyne-azide cycloaddition reaction (CuAAC or "click").[10] Chemical oxidation of the surface confined lactone moiety (**SAM-2**) to the corresponding benzoquinone acid was followed by its activation with carbodiimides and N-hydroxysuccinimide (**SAM-3**) to promote reactions of the exposed acid function toward nucleophiles. 3-Azidopropylamine **3a**, and 3-azidopropanol **3b** were attached to the activated construct via conventional amide coupling procedures (**SAM-4a** and **SAM-4b**, respectively). The redox-tagged switchable construct (**SAM-5a/-5b**) was prepared by CuAAC reactions between the azide-terminated surface **SAM-4a/4b** and ethynylferrocene **4**. Surface samples at all stages of modification were either characterized as is or electrochemically cleaved.

S1.4.1 Synthesis of ethynylferrocene (4)

Scheme S1. Synthesis of ethynylferrocene **4**

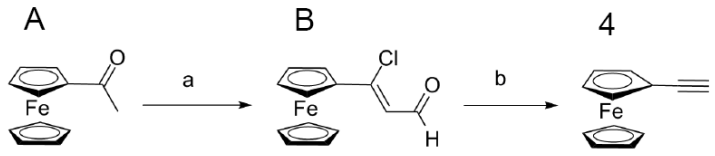

*(a) (2-Formyl-1-chlorovynyl)-ferrocene (**B**)*. A stirred solution of acetylferrocene **A** (456 mg, 2.01 mmol) in dry *N*,*N*-dimethylformamide (3.5 mL) was bubbled with argon for 20 min and then cooled to 0 °C on an ice bath. The solution was stirred for 5 min under an argon atmosphere while separately dry *N*,*N*-dimethylformamide (750 μL) was cooled on ice and phosphorus oxychloride (500 μL) was added to it under argon with mixing. The prepared complex was transferred dropwise with a cannula to the vigorously stirred solution of the ferrocene **A**. The addition was completed in 10 min and stirring was continued at 0 °C under argon for 2 h. Diethyl ether (7 mL) was added to the ice cold solution and the flask was fitted with a condenser. Anhydrous sodium acetate (1.5 g, 17.6 mmol) was added in one portion to the reaction mixture, followed by the addition of water (4 mL). The ice bath was removed and stirring was continued at room temperature for 1 h. Diethyl ether (10 mL) was then added to the solution before continuing the reaction for an additional 3 h at room temperature. The crude mixture was then poured into a separatory funnel and diluted with diethyl ether (30 mL) and water (10 mL). The organic layer was separated and the aqueous phase washed with diethyl ether (3 × 20 mL). The pooled organic phase was washed with saturated sodium bicarbonate solution (3 × 20 mL), water (3 × 20 mL), dried over Na_2SO_4, filtered and dried *in vacuo* to afford the crude ferrocene **B** as purple oil. The crude material was purified by silica gel column chromatography (ethyl acetate/light petroleum, 1:2) to afford the title compound **B** as a purple oil (146 mg, 27%) which was kept in the dark and used within 2 h as starting

material in the successive step. ^{1}H NMR (300 MHz, $CDCl_3$) δ: 10.09 (d, 1H, *J* = 6.0 Hz), 6.41 (d, 1H, *J* = 6.0 Hz), 4.86 (s, 2H), 4.56 (s, 2H), 4.21 (s, 5H).

*(b) Ethynylferrocene (**4**)*. A stirred solution of (2-formyl-1-chlorovinyl)-ferrocene **B** (105 mg, 0.38 mmol) in dry 1,4-dioxane (10 mL) was heated at 115 °C for 5 min under argon. A 1M sodium hydroxide solution (4 mL, 4 mmol) was added in one portion to the reaction mixture and stirring was continued at reflux for 25 min. The solution was allowed to cool to room temperature, poured onto ice (*ca*. 20 g) and then neutralized to pH *ca*. 7 by adding 3 M hydrochloric acid. The crude mixture was transferred into a separatory funnel and added with water (20 mL) and hexane (50mL). The organic phase was separated and washed with saturated $NaHCO_3$ solution (2 × 20 mL), water (2 × 20 mL), dried over Na_2SO_4, filtered and concentrated *in vacuo*. The crude residue was purified using column chromatography (light petroleum) to give the title compound as a dark orange solid (65 mg, 81%). ^{1}H NMR (300 MHz, $CDCl_3$) δ: 4.46 (t, 2H, *J* = 1.9 Hz), 4.21 (s, 5H), 4.19 (t, 2H, *J* = 1.9 Hz), 2.71 (s, 1H); ^{13}C NMR (75.5 MHz, $CDCl_3$) δ: 73.64, 71.90, 70.19, 68.86; IR (KBr, cm^{-1}): 3290, 3093, 2919, 2849, 2109, 1730, 1695, 1106, 1035, 1001, 915, 821.

S1.4.2 Surface modification

S1.4.2.1 Acetylene-termianted silicon(100) surface (SAM-1). Hydrosilylation of diyne **1** onto hydrogen-terminated Si(100) followed a previously reported procedure.[1, 2, 11] In brief, silicon wafers were cut into pieces (approx. 30 × 10 mm), and shards were cleaned in a 3:1 solution of concentrated sulfuric acid and 30% hydrogen peroxide for 30 min at 100 °C (CAUTION: this is a strong oxidant and reacts violently with organic substances). After cleaning and extensive water rinse, the silicon chips were immersed for 1.5 min in 2.5% aqueous hydrofluoric acid solution to passivate the silicon surface. This etching condition is known to create a mainly dihydride surface.[12] Samples were subsequently transferred to a

degassed (through a minimum of 4 freeze–pump–thaw cycles) sample of diyne **1**. The samples were kept under a stream of argon (H_2O < 10 ppb, O_2 < 5 ppb) while the reaction vessel was immersed in an oil bath set to 165 °C for 3 h. The flask was then opened to the atmosphere, and the functionalized surface samples (**SAM-1**) were rinsed several times with dichloromethane and rested for a 12-h period in a sealed vial under dichloromethane at +4 °C, before being either analyzed or further reacted with the redox linker molecule **2**.

S1.4.2.2 CuAAC attachment of the redox-switchable linker 2 onto the acetylenyl surface (SAM-2). To a reaction vial containing the alkyne-functionalized silicon surface (**SAM-1**) were added (i) the azide **2** (10 mM, 2-propanol/water, 2:1), (ii) copper(II) sulfate pentahydrate (0.8 mol% relative to the azide **2**) and (iii) sodium ascorbate (80 mol% relative to the azide **2**). Solvents were degassed before use. Reactions were carried out at 35 °C in the dark under an argon atmosphere,[13, 14] and stopped after 3 h by removal of the samples from the reaction vessel.[15] The prepared surface-bound [1,2,3]-triazoles (**SAM-2**) were rinsed consecutively with copious amounts of water and ethanol, and then rested at room temperature for a 1-min period in a 0.5 M hydrochloric acid solution. Samples were then rinsed with copious amounts water and ethanol before being either analyzed or further reacted.

S1.4.2.3 Oxidation of linker molecules to benzoquinone acids and their activation with NHS (SAM-3). Lactone-functionalized surface samples (**SAM-2**) were rinsed with tetrahydrofuran (*ca*. 50 mL) and then transferred to a mixture of tetrahydrofuran (6 mL) and water (3 mL). *N*-Bromosuccinimide (160 mg, 90 mmol) was added to the reaction vial and the solution agitated at room temperature in the dark for 1.5 h. The ring-opened,[16] benzoquinone acid intermediate was rinsed with water and tetrahydrofuran before being transferred to a reaction flask charged with *N*-(3-dimethylpropyl)-*N*'-ethylcarbodiimide hydrochloride (200 mg, 1.04 mmol) and *N*-hydroxysuccinimide (NHS, 240 mg, 2.09 mmol).

Water (10 mL) was added to the flask and the uncapped vessel shaken in the dark for 3 h at room temperature. Once removed from the reaction vessel, NHS-activated[17] samples (**SAM-3**) were washed with copious amounts of water and ethanol before being analyzed or further reacted.

S1.4.2.4 Nucleophilic substitutions at NHS-activated samples (SAM-4a and SAM-4b) Activated benzoquinone acid samples (**SAM-3**) were washed with *N*,*N*-dimethylformamide (*ca*. 20 mL), blown dry under a stream of argon and placed into a reaction tube containing either (i) 3-azidopropylamine **3a** (0.4 M) in *N*,*N*-dimethylformamide (5 mL) and of 4-*N*,*N*-(dimethylamino)pyridine (2.0 mg, 0.02 mmol) to give **SAM-4a**, or (ii) 3-azidopropanol **3b** (0.4 M) in *N*,*N*-dimethylformamide (10 mL) and 4-*N*,*N*-(dimethylamino)pyridine (2.0 mg, 0.02 mmol) to give **SAM-4b**. The reaction was continued at room temperature in the dark for 12 h and stopped by removing the silicon wafer from the reaction mixture. The putative azide-termianted samples were washed with *N*,*N*-dimethylformamide, ethanol and analyzed or further reacted.

S1.4.2.5 CuAAC attachment of ethynylferrocene 4 onto azide-terminated substrates (SAM-5). Ethnylferrocene **4** was covalently attached to terminal azido functionalities of **SAM-4a/-4b** *via* CuAAC reactions to yield ferrocene-tagged electrodes (**SAM-5a/-5b**, respectively). To a 20 mM solution of the ferrocene **4** in 2-propanol/water (2:1) relative to the acetylene were added (i) **SAM-4a** or **SAM-4b** samples, (ii) 0.4 mol% copper(II) sulfate pentahydrate and (iii) 40 mol% sodium ascorbate. Solvents were degassed before use and reactions were carried out at room temperature under an argon atmosphere and stopped after 1 h by removal of the modified sample from the reaction vessel. Modified silicon wafers were rinsed with copious amounts of water and ethanol and then rested for 1 min in a 0.5 M hydrochloric acid solution. Samples were then rinsed with copious amounts water and ethanol before being either analyzed or electrochemically cleaved.

S1.4.2.6 Electrochemical reduction of benzoquinone linkers

Cathodic bias to promote the benzoquinone reduction was applied either by means of cyclic voltammetry (CV) or in a potentiostatic fashion by imposing reductive potentials for defined time intervals. Kinetic data for the conversion, *i.e.*, switch, of **SAM-5** to its lactone precursor **SAM-2** were obtained combining potentiostatic and subsequent CV experiments. Switch experiments were performed varying: a) polarization times; b) electrolyte composition and c) substrate doping type. In general, once the circuit was open at the end of each potentiostatic run the electrolyte chamber was emptied and back-filled with fresh electrolyte solution before measuring changes in the observed ferrocene surface coverage, Γ, by means of cyclic voltammograms (CVs) in the 0/800 mV (p-type Si) or –100/200 mV (n-type, assisted by supra-band gap illumination) potential window.

S2. Passivation of the Si(100) surface with monolayers of 1,8-nonadiyne

XRR is a powerful tool for the investigation of self-assembled monolayers bound to silicon. It allows measuring the thickness (*d*) of such films with atomic resolution as a result of the fortunate high contrast in scattering length density (SLD)[18] of the organic molecules in the SAM (SLD ~1×10^{-5} Å^{-2}) compared to air (SLD = 0) and the silicon substrate (SLD = 2.01×10^{-5} Å^{-2}). The film thickness, in concert with the refined SLD, can also be used to establish the molecular foot-prints in the monolayer. The average surface roughness (σ) of these monolayers can also be precisely determined using this technique. Figure 1 shows the measured and refined XRR profiles for **SAM-1**. Our XRR-determined **SAM-1** film thickness of 9.6 Å is close to the 9–12 Å that was previously reported.[1, 2, 19] The symmetrical nature of diyne **1** opens no routes to alternative surface binding modes and XRR results show that polymerization of the terminal alkyne has not occurred, and that only one terminal C≡C triple bond of the diyne **1** has reacted with the surface. The electron density (ρ_{el}) of the organic layer was also derived from the XRR data and was found to be *ca*. 0.39 e^{-}/Å^3, consistent with previous reports of alkane- and alkyne-based SAMs, and supports the formation of a densely packed organic layer with very limited defects.[7, 20-22]

High-resolution Si 2p XPS spectra acquired on the acetylene-terminated **SAM-1** are shown in Fig. 2a. Independent of the doping type, the two refined spin–orbit-split contributions to the Si 2p doublet for the Si$^{(0)}$ oxidation state are located at 99.4 and 100.0 ± 0.2 eV.[23] Spectroscopic shifts for the Si 2p region introduced by Si$^{(1)}$–Si$^{(4)}$ oxides are well-documented.[24] The silicon oxide content (102–104 eV) was below the spectrometer detection limit; data supporting the high quality of the monolayer and its ability to prevent appreciable oxidation of the Si substrate. The high-resolution C 1s signal (Fig. 3a) was fitted with three component peaks; the major component at 285.0 eV (85%, 1.4 eV fwhm) is assigned to the methylene carbons of the adsorbate.[25] The lower binding energy component at 283.7 eV (6%,

1.0 eV fwhm) and the higher binding energy component at 286.4 eV (9%, 1.4 eV fwhm) are assigned to silicon-bound olefinic carbons (silylated olefin, Si–C=C)[25, 26] and to either oxygen-bound carbon atoms (C–O),[1, 27] or sp-hybridized carbon-bound carbon, respectively.[28] On hydrogenated silicon surfaces, the assembly of monolayers of 1-alkynes is likely to result in sp^2 hybridization at the surface. The growth of sp^2 structures is kinetically more facile than that of sp^3 structures (*i.e.*, 1-alkene adsorbates),[29-31] possibly by a factor of up to 6:1.[32] This is important because in the former case the Si–C=C linkage of an alkenyl monolayer is known to inhibit oxidation of the underlying silicon and enhance the monolayer stability.[2, 33] π-Conjugation near the surface has also been shown to facilitate charge transport by improving electronic coupling,[31] and is therefore desirable for electrochemical sensing,[19, 34] bioelectronics,[35] and for electronic applications of molecular adsorbates on semiconductors.[36]

XPS data does support the existence of some oxidized carbon in the film, and this is in line with entropic considerations.[37] The C 1s peak decomposition may indicate that a non-negligible number of C–O bonds exist in monolayers of diyne **1**. The structure of the adventitious C–O bond is still highly debated, although contamination has been reported in several studies.[25, 27, 37, 38] For instance, Kramer and co-workers suggests that a shift from 285 to 286.5 eV is likely to be associated to the core ionization of monohydroxyl carbon atoms (–Si–CHC(OH)–).[38] More recently, Zuilhof and co-workers have suggested that the emission at 286.5 eV may also include emissions from –C≡C– groups.[28] Signals from the deconvoluted O 1s signal (Fig. S4a) may clarify the origin of this high binding energy C 1s feature. The large width and asymmetric shape of the O 1s emission indicates that there is more than one type of oxygen adsorbed on the surface, and the spectra can be divided into two components with energies of 532.0 and 533.1 eV. On the basis of electronegativity considerations the O 1s

peak at *ca*. 533 eV can be attributed to the oxygen of the free alcohol, while the peak at *ca*. 532 eV to the oxygen of water adsorbates.[39]

The atomic $C_{286.4}$ 1s/O_{533} 1s ratio was 1.2 ± 0.2 (95% confidence limit of the mean calculated as $t_{n-1}\ s/n^{1/2}$ where t_{n-1} = 2.23[40]), a value which approaches very close to unity if one takes into account differences in attenuation lengths values through hydrocarbon films for O 1s and C 1s photoelectrons (1.3:1 ratio between $\lambda_{C,ML}$ and $\lambda_{O,ML}$[41]). This data leads us to refine further the hypotheses of the origin of the $C_{286.4}$ 1s signal. That is, without entirely ruling out the possibility of –C≡C– emissions contributing to the 286.5 eV envelope,[28] however, our data would more strongly support the model of Kramer and co-workers,[38] where the hydrosilylation of 1-alkynes occurs with partial oxidation of the proximal silylated olefin function.

It needs to be noted that the intensity ratio between the low- and high-binding energy O 1s contributions varied greatly between samples, ranging from *ca*. 1.8 to *ca*. 4.3 (Fig. S4a). These measurements indicate that despite the rinsing of the samples with low dielectric solvents (*i.e.*, dichloromethane) and despite the low pressure in the XPS analysis chamber, minor amounts of physisorbed water are not easily removed even from relatively hydrophobic films.[42-44]

S3. 'Click' Attachment of the Redox-sensitive Linker Molecule 2 (SAM-2)

The XPS C 1s signal for **SAM-2** samples was deconvoluted with fitting to four functions: i) carbon in a carbide configuration (Si–C) at 283.7 eV), ii) a main contribution centred at 285 eV ascribed to aliphatic and aromatic carbon-bonded carbon (C−C)[25, 45]; iii) a signal at 286.4 eV corresponding to nitrogen-, oxygen-, and carbonyl-bonded carbon (C−N,[1] C−O,[46] and C(O)C)[47]), data which further supports the formation of **SAM-2**; and iv) a high-binding energy signal at 289.3 eV assigned to the electron-deficient carbon atom in the lactone carbonyl group (O−C=O).[48, 49] In Fig. S4b, the main contribution of O 1s (*ca*. 532 eV) still

originates from the oxygen in water adsorbates (see §S2), however, the O 1s spectrum now shows a clear component centered at 533.9 eV. This high binding energy feature presumably originates from the lactone moiety (O–C(O)), but a more precise deconvolution of the O 1s signal is difficult and we cannot rule out a contribution to this component from partially hydroxylated silylated olefins.[38, 50]

S4. Additional spectroscopic and electrochemical data

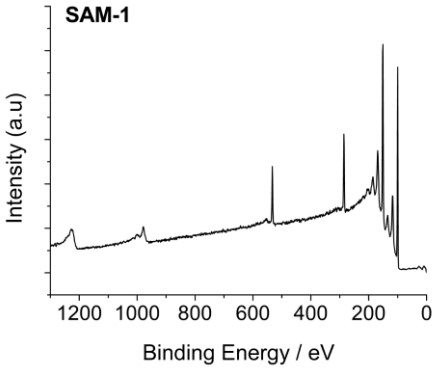

Figure S1. Survey XPS spectra for **SAM-1** samples.

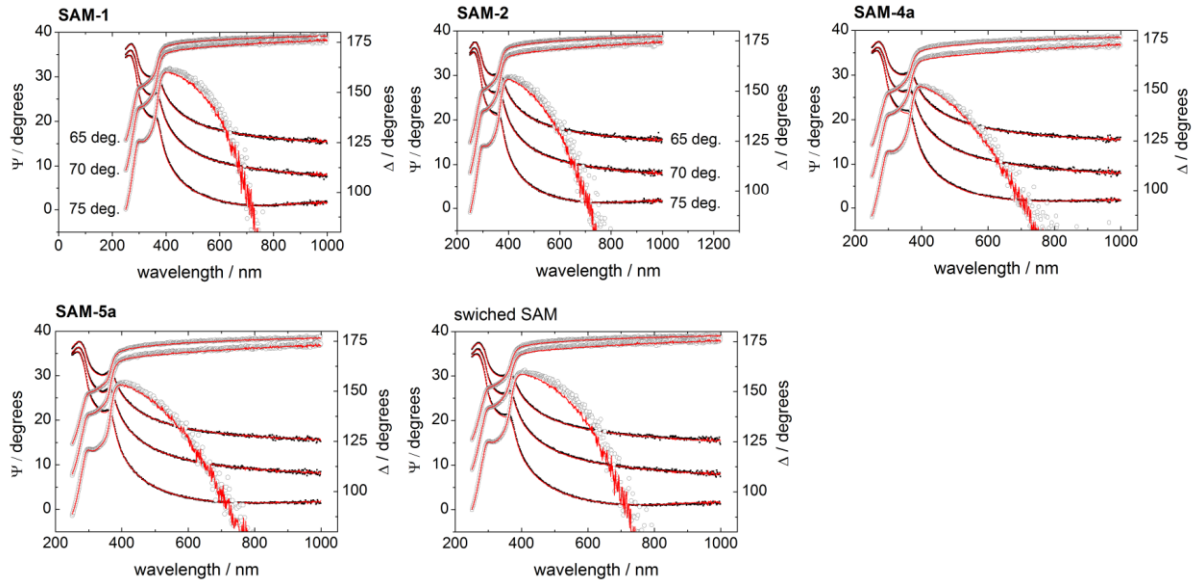

Figure S2. Experimental Ψ (●) and Δ (○) data and best-fit models (—) for spectroscopic ellipsometry measurements of the surfaces in Scheme 2 (see main text). The incidence angles were 65, 70 and 75° (graphs from top toward bottom). Ellipsometry determines the complex reflectance ratio $\rho = r_s / r_p = \tan \Psi \exp(i\Delta)$, where r_P and r_S are the Fresnel reflection coefficients for light polarized parallel and perpendicular to the plane of incidence, respectively. The angle Ψ is the ratio of the changes in amplitude for the s and p polarizations after reflection. The angle Δ relates to the difference in the phase shift after reflection for the two polarizations.

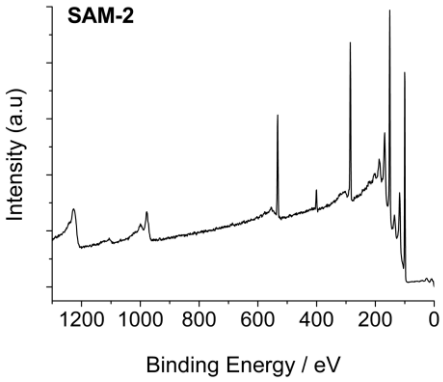

Figure S3. Survey XPS spectra for **SAM-2** samples.

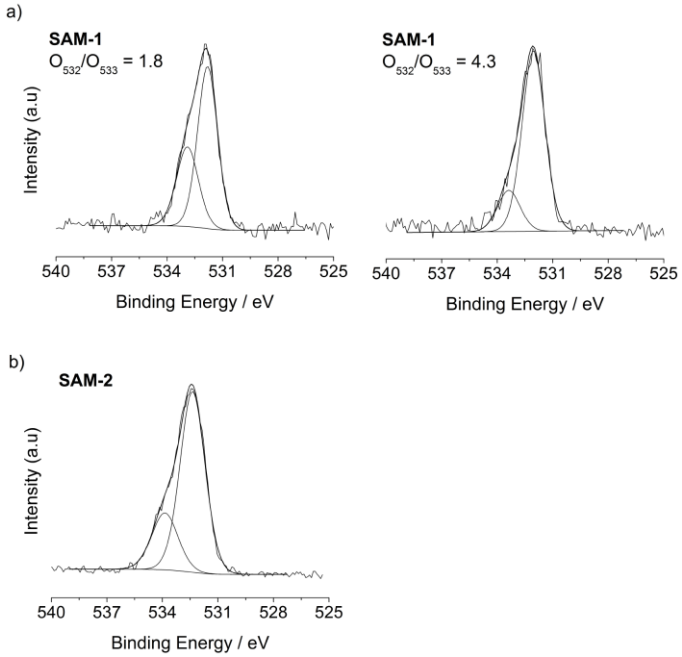

Figure S4. O 1s narrow scans for **SAM-1** (a), and **SAM-2** (b) samples.

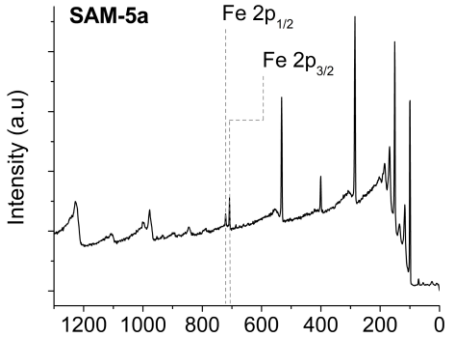

Figure S5. Survey XPS spectra for **SAM-5a** samples.

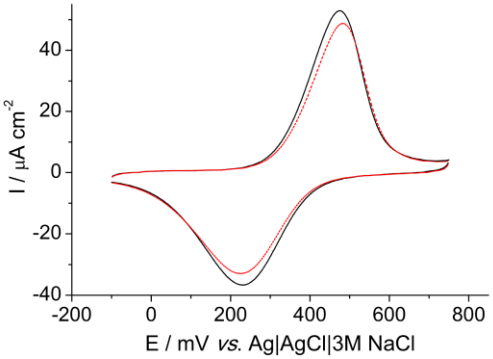

Figure S6. Representative cyclic voltammograms (ν = 500 mV s^{-1}) for **SAM-5a** samples before (black solid line) and upon (red dashed line) prolonged cyclic voltammetry analysis (100 cycles) in 1.0 M $HClO_4$ electrolytes. The measured ferrocene coverage, Γ, decreased to 1.63×10^{-10} mol cm^{-2} from 1.72×10^{-10} mol cm^{-2} and fwhm was unaltered at 152 mV.

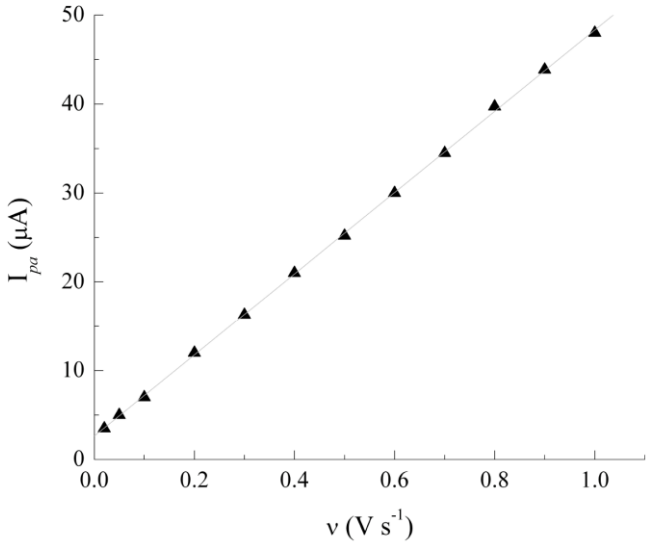

Figure S7. Linear dependence of the anodic peak current on the scan rate (ν) for ethynylferrocene **4**-functionalized Si(100) electrodes (**SAM-5a**).

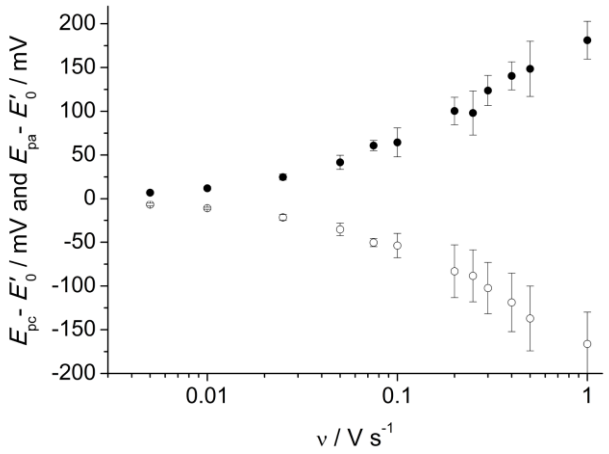

Figure S8. Dependence of ΔE_p on ν values for CV data of **SAM-5a** samples. With increasing scan rates E_{pc} (○) and E_{pa} (●) diverged similarly from the E'_0 value extrapolated from voltammograms taken at low scan rates.

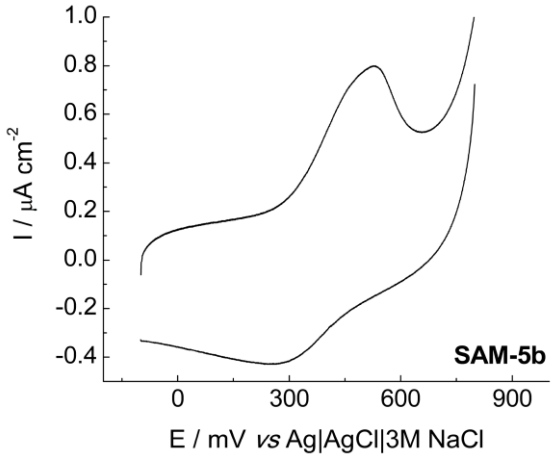

Figure S9. Cyclic voltammogram in 0.1 M $NaClO_4$ (pH 7) of ethynylferrocene **4**-modified electrodes (**SAM-5b**) prepared from the *ester* construct **SAM-4b**. Scan rate was 0.1 V s^{-1}. For voltammograms at low scan rates, large dispersion values (184 mV fwhm) and ΔE_p greater than 200 mV were observed for **SAM-5b**. This far from ideal redox behaviour was interpreted as a poorly defined electrode surface, where lack of rigidity combined with very low Γ values might have lead to ferrocenyl groups being allowed to interact strongly with the surrounding alkane-like environment and thus accounting for a reduced ion-pairing capability. It is not yet clear, however, if the reported low Γ values were solely due to poor yields for the nucleophilic substitution reaction at the carbonyl (C=O) of the activated construct **SAM-3** with the alcohol 3-azidopropanol **3b**. Nevertheless, this suggestion would agree with the notion of increased nucleophilicity of primary amines relative to primary alcohols, and explain greater yields, leading to *ca*. 20-fold larger Γ values, observed for the analogous substitution reaction when 3-azidopropylamine **3a** is reacted in place of alcohol **3b** with **SAM-3**.

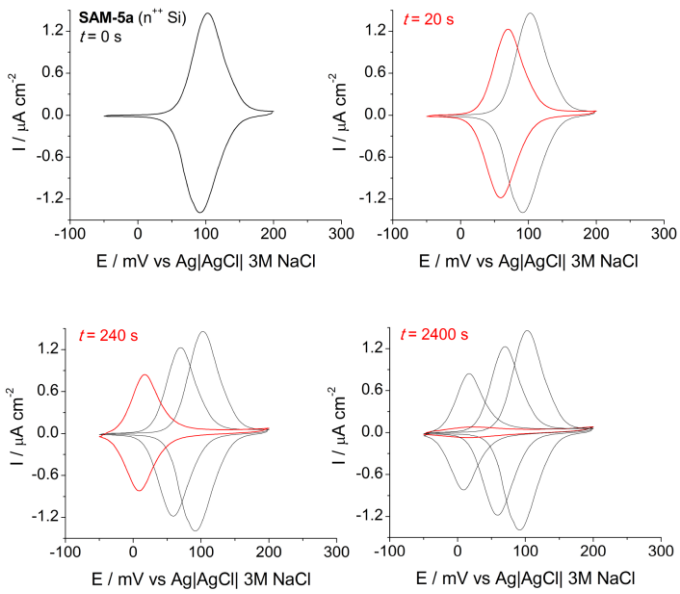

Figure S10. Electrochemical reduction of **SAM-5a** n^{++} electrodes under cathodic bias (–900 mV) in 1.0 M $HClO_4$ under diffuse ambient illumination. Cathodic reduction of **SAM-5a** to **SAM-2** was close to completion after ca. 2400 s of total polarization time, as judged from a decline in the ferrocene faradic signal of CVs acquired between successive potentiostatic experiments. The scan rate in CV runs was 5 mV s^{-1}. For instance, a 20% extent of conversion to the lactonized construct (**SAM-2**) is observed after *ca*. 20 s of reaction time. Conversion is close to 45% after 240 s and quantitative after 2400 s. CV runs to monitor the course of Γ values with polarization times were acquired under supra-bang gap illumination of the Si electrode (642 nm, ~20 mW).

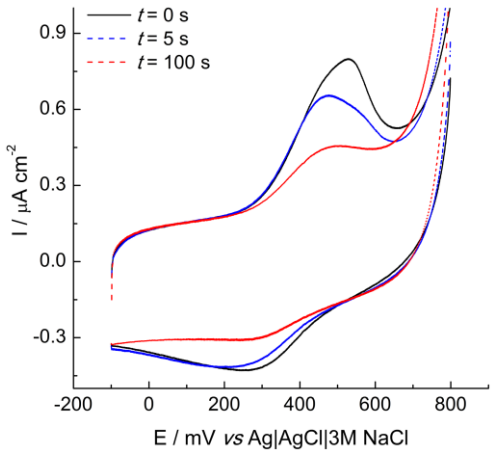

Figure S11. Electrochemical reduction (–900 mV) of redox constructs incorporating an *ester* link (surface **SAM-5b**). CVs (ν = 100 mV s^{-1}) were acquired prior to (t = 0 s) and at defined times (t = 5, 100 s) during the cleavage of tethered **4** derivatives. After 100 s of total polarization time the measured ferrocene coverage, Γ, decreased to 2.01 × 10^{-12} mol cm^{-2} from 7.88 × 10^{-12} mol cm^{-2} (*ca*. 75% conversion to **SAM-2**).

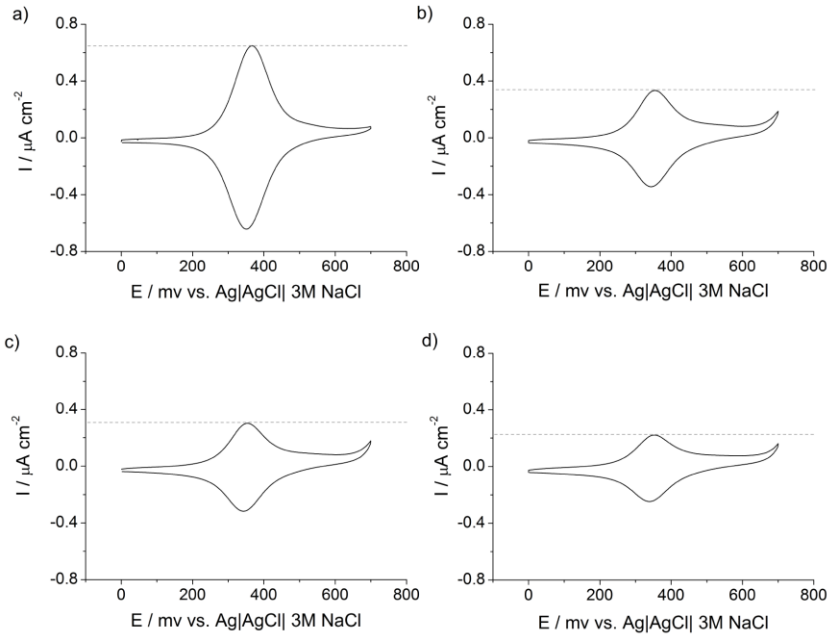

Figure S12. Representative cyclic voltammograms for electrochemically switched silicon electrodes (**SAM-5a→SAM-2**). A reducing potential was created at the working silicon electrode (–1400 mV vs ref.) and the electrochemical circuit was opened for a specified time (*t*) ((a), *t* = 0 s; (b), *t* = 5 s; (c), *t* = 10 s; (d), *t* = 30 s). After 30 s of total polarization time the measured ferrocene coverage, Γ, decreased to 5.09×10^{-11} mol cm^{-2} from 1.67×10^{-10} mol cm^{-2} (*ca*. 30% conversion to **SAM-2**). Peak fwhm and ΔE_p values were unaltered with polarization times *t*. CVs were acquired in 1.0 M $HClO_4$ (ν = 5 mV s^{-1}).

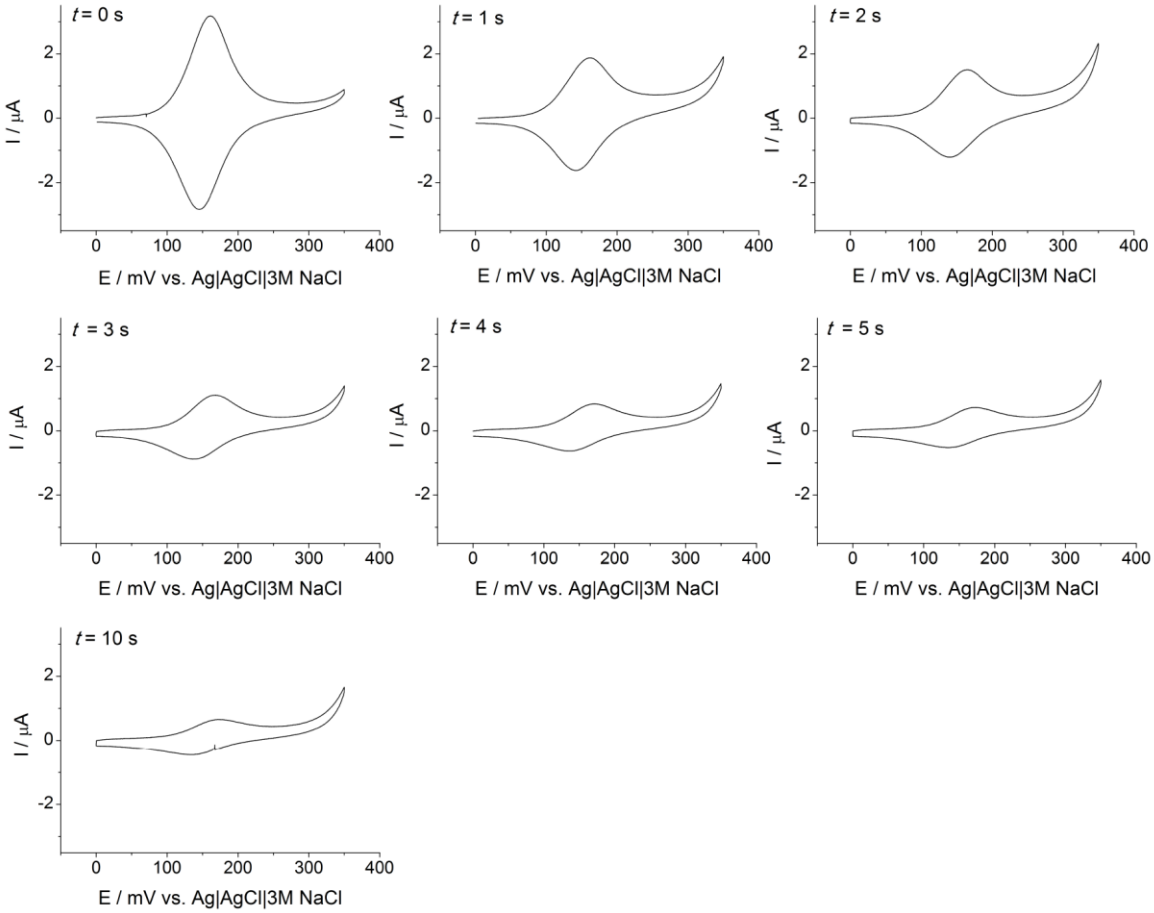

Figure S13. Electrochemical reduction of **SAM-5a** electrodes under cathodic bias (–1800 mV *vs* ref.) in 1.0 M $NaClO_4$ (pH 7). Cathodic reduction of **SAM-5a** to **SAM-2** was close to completion after *ca*. 10 s of total polarization time, as judged from a decline in the ferrocene faradic signal of CVs acquired between successive potentiostatic experiments. Experiments were performed under diffuse ambient illumination. After 10 s of total polarization time the measured ferrocene coverage, Γ, decreased to 1.17×10^{-11} mol cm^{-2} (t = 10 s) from 8.59×10^{-11} mol cm^{-2} (t = 0 s). Peak fwhm and peak positions were unchangenged with with polarization time ($E^{'}_{0}$ = 306 mV, E_{fwhm} = 320 mV). CVs were acquired at ν = 5 mV s^{-1}.

Note to Figure S13. Quinone derivatives have pH-dependent redox behavior,[51] and therefore the electrolyte pH was expected to have a tangible effect on the electrochemically-driven release of ferrocene **4** derivatives, with a slower switch expected at higher pH values. As a proof-of-principle such an effect was investigated for **SAM-5a** by performing the electrochemical sequence of above in perchlorate-containing solutions buffered at pH 7. As judged by means of voltammetric analysis (Fig. S13) it was not possible to observe differences between reactions performed in perchloric acid or in sodium perchlorate (pH 7) electrolytes. Interestingly, a *ca*. 50 mV increase in the E'_0 value is observed in acidic $HClO_4$ electrolyte compared to pH 7 $NaClO_4$. As the chemical composition of the film was unaltered, the shifts for E'_0 toward more positive values indicate a reduction process becoming energetically more favorable. It is proposed that the observed positive shifts in the apparent formal potential values could be attributed to either one or a combination of the following i) in an acidic media the

positively charged ferricenium form of the redox couple is progressively destabilized relatively to the uncharged ferrocene counterpart, and ii) favored conjugation of the ferrocenyl groups in the oxidized form with neighboring [1,2,3]-triazole rings. The former would call for molecules in the film bearing a net positive charge at low pH values, thus repelling terminal oxidized ferricenium units.

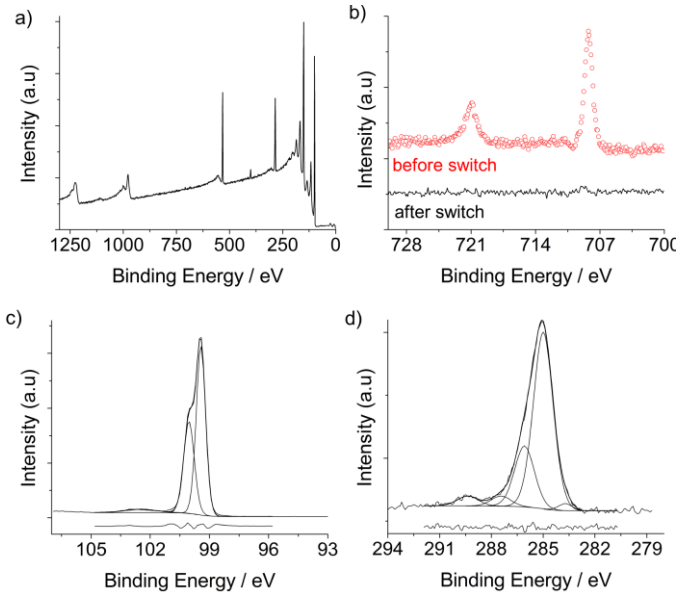

Figure S14. XPS analysis for switched electrodes (**SAM-5a→SAM-2**). (a) Survey scan, (b) Fe 2p region, (c) Si 2p with approx. 0.2 SiO_x fractional monolayer equivalents, and (d) C 1s with refined Si–C (283.7 eV), C−C (285 eV), C−N C−O, and C(O)C (287.4 eV) and O−C=O (289.4 eV) features.

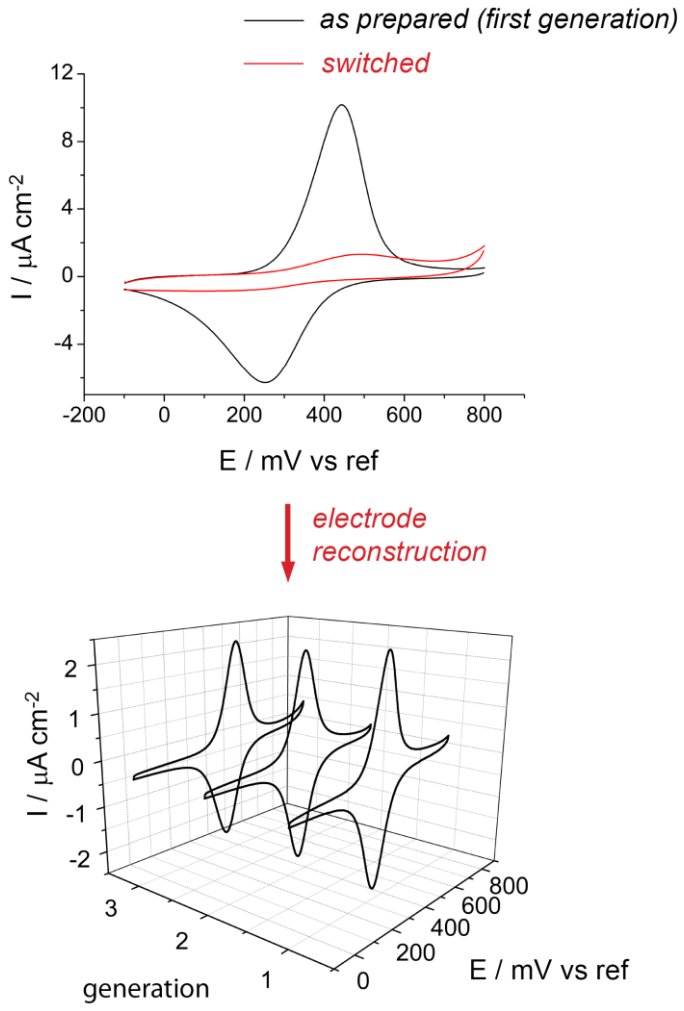

Figure S15. Representative cyclic voltammograms (CVs) for the electrochemical switch and subseequent electrode regeneration. The top panel shows CVs (ν = 20 mV s^{-1}, 1.0 M $HClO_4$) for as prepared **SAM-5a** electrodes (Γ = 1.71 × 10^{-10} mol cm^{-2}, *first generation*) and after (Γ =1.09 × 10^{-11} mol cm^{-2}) the electrochemical cleavage sequence of Scheme 1. Electrodes regenerated by chemical means (Scheme 2) up to two times (3rd generation electrodes) displayed redox performances with only marginal deviations from their precursors (bottom panel; $\Gamma_{\text{first generation}}$ = 1.71 × 10^{-10} mol cm^{-2}, $\Gamma_{\text{second generation}}$ = 1.63 × 10^{-10} mol cm^{-2} $\Gamma_{\text{third generation}}$ = 1.48 × 10^{-10} mol cm^{-2}, k^0_{et} (from CV methods) and $E^{'}_0$ values were 0.7 s^{-1}/361 mV, 0.9 s^{-1}/370 mV and 0.4 s^{-1}/368 mV for first, second and third generation electrodes, respectively).

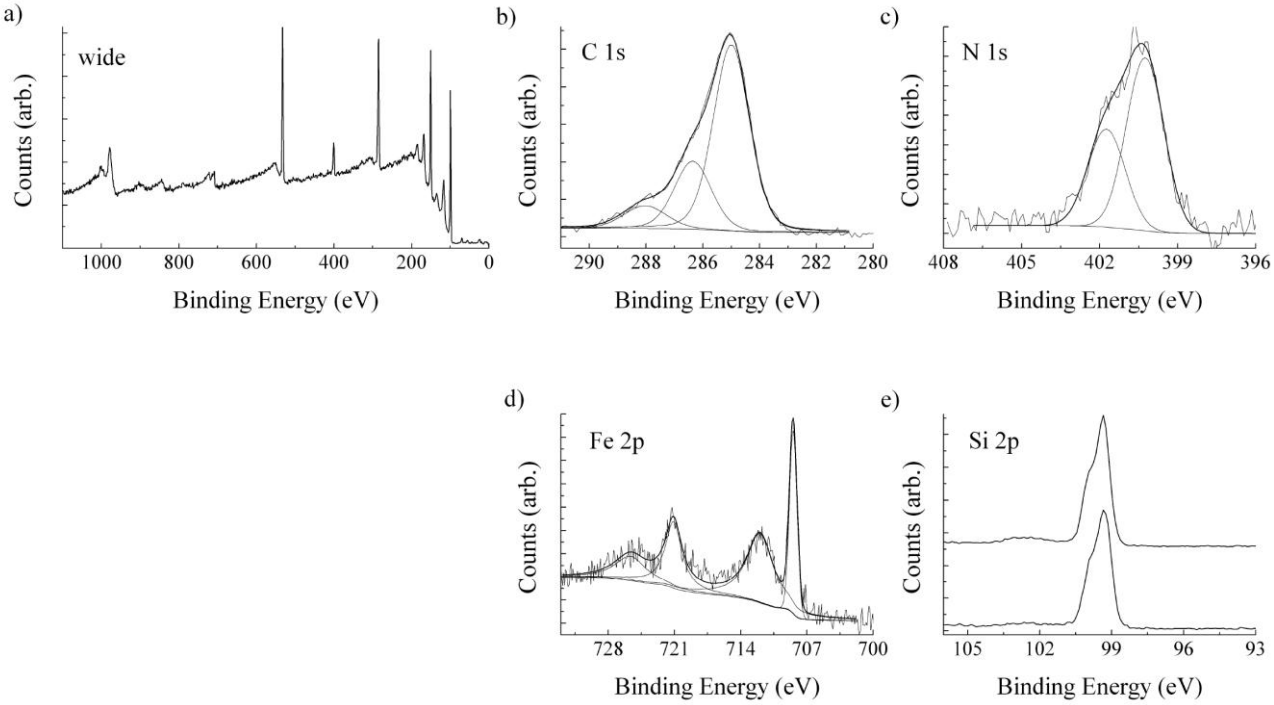

Figure S16. Survey (a) and high-resolution C 1s, N 1s and Fe 2p XPS (b–d) scans for regenerated, third generation, ferrocene-terminated **SAM-5a** surfaces. Panel (e) shows Si 2p narrow scans for second generation (lower spectra) and third generation (upper spectra) electrodes with fractional silicon oxide coverage estimated to *ca*. 0.1 and *ca*. 0.3 monolayers, respectively.

Table S1. Representative XPS data for modified Si(100) surfaces[a,b,c]

monolayer structure	BE (eV)						
SAM-1	C−C	C−O			Si −C		
	285.0 (1.4)[d]	286.4 (1.4)			283.7 (1.0)		
SAM-2	C−C	C−O/−N, C(O)C	O−C=O		Si −C		N
	285.0 (1.4)	286.4 (1.4)	289.3 (0.8)		283.7 (1.0)		401.7 (1.4)
							400.3 (1.4)
SAM-4a	C−C	C−O/−N, C(O)C	C=O	N−C(O)	Si −C		N
	285.0 (1.5)	286.3 (1.3)	287.7 (1.5)	289.3 (0.7)	283.9 (0.9)		404.6 (1.0)
							401.4 (1.5)
							400.2 (1.7)
SAM-5a	C−C	C−O/−N, C(O)C	C=O	N−C(O)	Si −C	Fe[e]	N
	285.0 (1.4)	286.2 (1.4)	287.9 (1.3)	289.3 (0.8)	283.6 (1.0)	708.2 (1.1)	401.6 (1.4)
						721.0 (1.7)	400.2 (1.4)

monolayer structure	XPS atomic ratio[f] / stoichiometric ratio[g]		
SAM-2	C−C:N[h]	O−C=O:(C−O/−N, C(O)C)	O−C=O:N[h]
	8.4:1/—	0.8:6/1:6	1.2:3/1:3
SAM-4a	N_{405}:N[h]	N−C(O):N_{405}	N[h]:C=O
	0.7:6/1:6	0.8:1/1:1	3.1:2/6:2
SAM-5a	N−C(O):Fe[i]	C=O:C−N/C(O)C	C=O:Fe[i]
	0.8:1/1:1	2.1:6/1:6	5.2:1/3:1

[a] all entries refers to data for fitted functions. Optimized Lorentzian-Gaussian combination used in fitting routines of individual elements have been previously reported[1]
[b] data for freshly prepared samples, prior to chemical/electrochemical cleaving procedures
[c] for a list of abbreviations used in tables refer to main text
[d] fwhm for the fitted functions are in parentheses
[e] narrow scan of the Fe 2p region comprised the two spin-orbit split components 3/2 and 1/2 found at *ca*. 708 and ca. 721 eV, respectively, and no high-binding energy satellite signals at *ca*. 712 and *ca*. 725 eV, generally associated to Fe(III)-related compounds
[f] relative atomic ratios were measured from relative XPS intensity ratios after normalization for atomic sensitivity factors, scanning time and for a square root dependence on the photoelectron kinetic energy
[g] calculated for the putative product surface
[h] total N 1s signal in the 399−402 eV region
[i] total Fe 2p signal in the 706–726 eV region

References

1. S. Ciampi, T. Böcking, K. A. Kilian, M. James, J. B. Harper and J. J. Gooding, *Langmuir*, 2007, **23**, 9320-9329.
2. S. Ciampi, P. K. Eggers, G. Le Saux, M. James, J. B. Harper and J. J. Gooding, *Langmuir*, 2009, **25**, 2530-2539.
3. L. J. Webb and N. S. Lewis, *J. Phys. Chem. B*, 2003, **107**, 5404-5412.
4. A. Nelson, *J. Appl. Crystallogr.* , 2006, **39**, 273-276.
5. E. Laviron, *J. Electroanal. Chem.* , 1979, **97**, 135-149.
6. S. Ciampi, M. James, G. Le Saux, K. Gaus and J. Justin Gooding, *J. Am. Chem. Soc.*, 2012, **134**, 844-847.
7. M. James, S. Ciampi, T. A. Darwish, T. L. Hanley, S. O. Sylvester and J. J. Gooding, *Langmuir*, 2011, **27**, 10753-10762.
8. M. Rosenblum, N. Brawn, J. Papenmeier and M. Applebaum, *J. Organomet. Chem.*, 1966, **6**, 173-180.
9. Chemical oxidation of the confined lactone **2** leads to the exposure of a carboxylic acid functionality amenable to further derivatization.
10. M. Meldal and C. W. Tornøe, *Chem. Rev.*, 2008, **108**, 2952-3015.
11. S. Ciampi, G. Le Saux, J. B. Harper and J. J. Gooding, *Electroanalysis*, 2008, **20**, 1513-1519.
12. Y. J. Chabal, G. S. Higashi, K. Raghavachari and V. A. Burrows, *J. Vac. Sci. Technol. A*, 1989, **7**, 2104-2109.
13. G. Qin, C. Santos, W. Zhang, Y. Li, A. Kumar, U. J. Erasquin, K. Liu, P. Muradov, B. W. Trautner and C. Cai, *J. Am. Chem. Soc.*, 2010, **132**, 16432–16441.
14. A. Kumar, K. Li and C. Cai, *Chem. Commun.*, 2011, **47**, 3186-3188.
15. The unreacted lactone **2** used in surface modification procedures was routinely recovered and purified via column chromatography (ethyl acetate/light petroleum, 1:2).
16. A. Zheng, D. Shan and B. Wang, *J. Org. Chem.* , 1999, **64**, 156-161.
17. V. G. Janolino and H. E. Swaisgood, *Biotechnol. Bioeng.*, 1982, **24**, 1069-1080.
18. SLD for X-rays is obtained by multiplying the electron density (e-/Å3) of the material by the factor 2.82 × 10-5 Å.
19. F. Shamsi, H. Coster and K. A. Jolliffe, *Surf. Sci.*, 2011, **605**, 1763-1770.
20. M. R. Linford, P. Fenter, P. M. Eisenberger and C. E. D. Chidsey, *J. Am. Chem. Soc.*, 1995, **117**, 3145-3155.
21. T. Böcking, M. James, H. G. L. Coster, T. C. Chilcott and K. D. Barrow, *Langmuir*, 2004, **20**, 9227-9235.
22. H. Jin, C. R. Kinser, P. A. Bertin, D. E. Kramer, J. A. Libera, M. C. Hersam, S. T. Nguyen and M. J. Bedzyk, *Langmuir*, 2004, **20**, 6252-6258.
23. For the case of non-degenerated silicon, the position of the low-binding energy Si 2p contribution (Si $2p_{3/2}$) could be used to obtain information on the effect the monolayer formation has on band bending (S. p. Cordier, B. Fabre, Y. Molard, A.-B. Fadjie-Djomkam, N. Tournerie, A. Ledneva, N. G. Naumov, A. Moreac, P. Turban, S. Tricot, S. Ababou-Girard and C. Godet, *J. Phys. Chem. C*, 2010, **114**, 18622-18633) and/or to probe any masking of these effects by surface states (i.e. Fermi level pinning).
24. F. J. Himpsel, F. R. McFeely, A. Taleb-Ibrahimi, J. A. Yarmoff and G. Hollinger, *Phys. Rev. B*, 1988, **38**, 6084-6096.
25. X. Wallart, C. H. de Villeneuve and P. Allongue, *J. Am. Chem. Soc.* , 2005, **127**, 7871-7878.
26. H. Liu and R. J. Hamers, *Surf. Sci.*, 1998, **416**, 354-362.
27. L. Scheres, A. Arafat and H. Zuilhof, *Langmuir*, 2007, **23**, 8343-8346.
28. B. Rijksen, S. P. Pujari, L. Scheres, C. J. M. van Rijn, J. E. Baio, T. Weidner and H. Zuilhof, *Langmuir*, 2012, **28**, 6577-6588.
29. A. Ng, S. Ciampi, M. James, J. B. Harper and J. J. Gooding, *Langmuir*, 2009, **25**, 13934-13941.
30. J.-H. Lee, J.-H. Choi and J.-H. Cho, *J. Phys. Chem. C*, 2011, **115**, 14942-14946.
31. M. A. Walsh, S. R. Walter, K. H. Bevan, F. M. Geiger and M. C. Hersam, *J. Am. Chem. Soc.*, 2010, **132**, 3013-3019.
32. B. Rijksen, B. van Lagen and H. Zuilhof, *J. Am. Chem. Soc.*, 2011, **133**, 4998-5008.
33. S. R. Puniredd, O. Assad and H. Haick, *J. Am. Chem. Soc.*, 2008, **130**, 13727-13734.
34. S. Ciampi, M. James, P. Michaels and J. J. Gooding, *Langmuir*, 2011, **27**, 6940-6949.
35. S. Ciampi and J. J. Gooding, *Chem. Eur. J.*, 2010, **16**, 5961-5968.
36. Y. Li, S. Calder, O. Yaffe, D. Cahen, H. Haick, L. Kronik and H. Zuilhof, *Langmuir*, 2012, **28**, 9920-9929.
37. G. F. Cerofolini, C. Galati, S. Reina and L. Renna, *Surf. Interface Anal.*, 2006, **38**, 126-138.
38. M. Kondo, T. E. Mates, D. A. Fischer, F. Wudl and E. J. Kramer, *Langmuir*, 2010, **26**, 17000-17012.

39. Y. L. Zhong and S. L. Bernasek, *Langmuir*, 2011, **27**, 1796-1802.
40. J. N. Miller and J. C. Miller, *Statistics and Chemometrics for Analytical Chemistry*, Prentice Hall, 2000.
41. C. D. Bain and G. M. Whitesides, *J. Phys. Chem.*, 1989, **93**, 1670-1673.
42. J. E. Baio, T. Weidner, J. Brison, D. J. Graham, L. J. Gamble and D. G. Castner, *J. Electron Spectrosc. Relat. Phenom.*, 2009, **172**, 2-8.
43. M. James, T. A. Darwish, S. Ciampi, S. O. Sylvester, Z. Zhang, A. Ng, J. J. Gooding and T. L. Hanley, *Soft Matter*, 2011, **7**, 5309-5318.
44. N. Clément, D. Guérin, S. Pleutin, S. Godey and D. Vuillaume, *J. Phys. Chem. C*, 2012, **116**, 17753-17763.
45. A. Lehner, G. Steinhoff, M. S. Brandt, M. Eickhoff and M. Stutzmann, *J. Appl. Phys.*, 2003, **94**, 2289-2294.
46. M. Yang, D. Wouters, M. Giesbers, U. S. Schubert and H. Zuilhof, *ACS Nano*, 2009, **3**, 2887-2900.
47. Y. L. Zhong and S. L. Bernasek, *J. Am. Chem. Soc.*, 2011, **133**, 8118-8121.
48. T. Strother, W. Cai, X. Zhao, R. J. Hamers and L. M. Smith, *J. Am. Chem. Soc.*, 2000, **122**, 1205-1209.
49. D. Briggs and M. P. Seah, *Practical Surface Analysis by Auger and X-ray Photoelectron Spectroscopy*, Wiley, Chichester, U.K., **1983**.
50. G. P. López, D. G. Castner and B. D. Ratner, *Surf. Interface Anal.*, 1991, **17**, 267-272.
51. Y. Sato, M. Fujita, F. Mizutani and K. Uosaki, *J. Electroanal. Chem.* , 1996, **409**, 145-154.